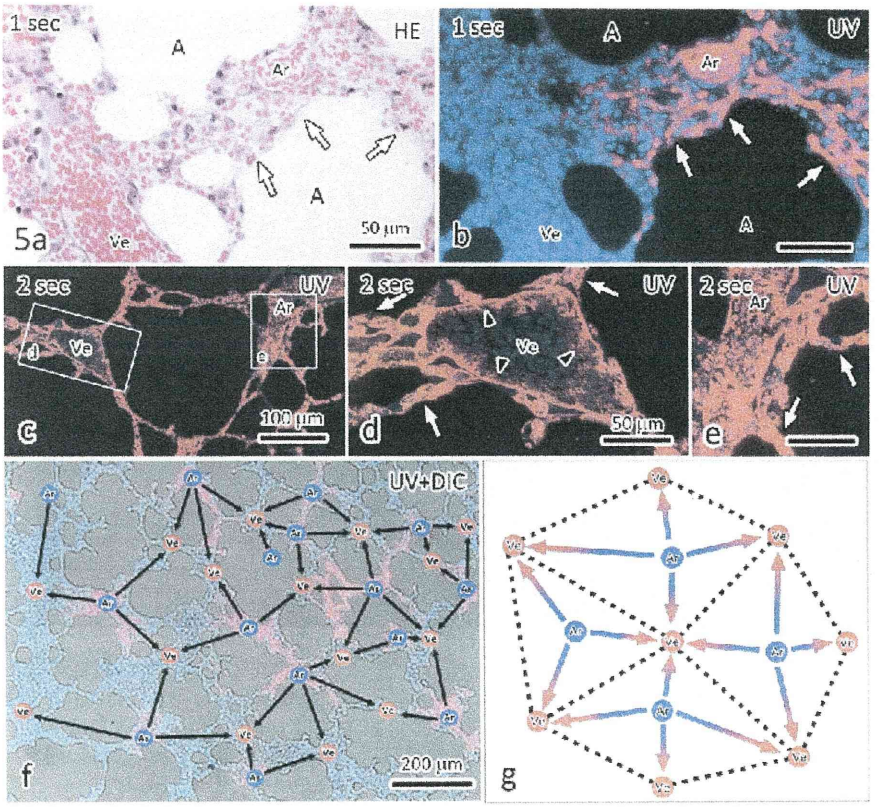

図5. Qdot注入1秒(a, b)および2秒(c-e)後に生体内凍結した肺組織のHE染色像(a)と紫外線励起した蛍光像(b-e).
(d, e)は(c)の一部拡大.
(b, d, e)矢印はQdotが流入した肺胞中隔壁内毛細血管を示す.
(f, g)は,得られたQdotの分布を模式図化したもの.隣接する細動静脈間での血行動態がQdotの蛍光として切片上に確認できる.隣接する細動脈を取り囲むように細静脈が配置されている(gの点線).
Ar:細動脈,Ve:細静脈.

顕用切片上で観察できていることになる(図5f, g)。

3. 共焦点レーザー走査型顕微鏡による肺胞中隔壁の三次元的再構築像

さらに呼吸時の肺胞中隔壁の立体構造を観察するためには,この生体内凍結－凍結置換固定したQdot注入肺組織ブロック試料を,比較的厚い切片のまま(約42 μm)で脱パラフィンしてスライドガラスに封入した。さらに共焦点レーザー走査型顕微鏡を用いて,Z軸方向の光学的切片(0.39 μm)より約100枚の画像情報を得ることができ,その連続した光学的切片像をコンピューター処置により,三次元再構築した。そこで,右心室注入2秒後での肺胞中隔壁毛細血管内Qdotは,紫外線励起による赤色蛍光を発して,肺胞中隔壁の組織成分は,自家蛍光の青色で同定できるため,肺胞中隔壁内毛細血管網の立体的形態像が得られた(図6d)。この立体的デジタル再構築像は,コンピューター画像処理により,任意の断面像を確認できる(図6e)。

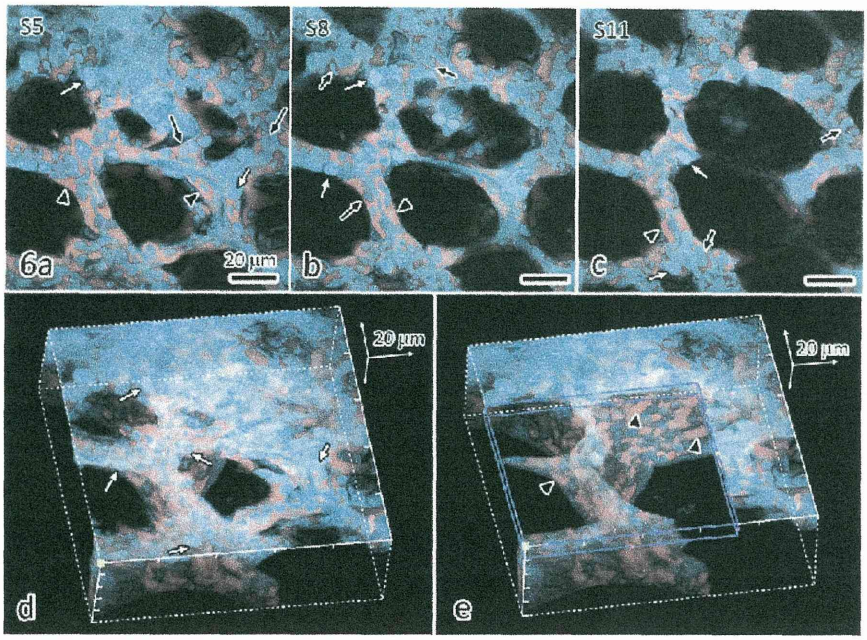

図 6. 共焦点レーザー走査型顕微鏡による Qdot 注入後に生体内凍結した肺組織の立体再構築像：光学切片像 108 枚中の 5 枚目（a），8 枚目（b），11 枚目（c）と立体再構築像（d）を示す．肺胞中隔壁の自家蛍光は青色，Qdot の蛍光は赤色で示す．Qdot の流入した肺胞中隔壁内毛細血管が明瞭に認められ，血管内を流れる赤血球や白血球も自家蛍光により区別できる．
(e) 立体再構築像の任意の断面像（青線）を得られる．
矢頭：Qdot の流入した肺胞毛細血管．
黒矢印（➡）：様々な形状の赤血球．
白矢印（⇒）：様々な形状の白血球．

IV. 実験的肺水腫モデルでの血清蛋白局在の可視化

実験的肺高血圧下マウスの肺組織では，肺胞中隔壁の形態は保たれていたが，赤血球がうっ滞する毛細血管や，肺胞中隔壁内および終末細気管支周囲の壊れた結合組織，さらに肺胞腔内に充満するエオジン好性漏出液を認めた。さらにアザン染色およびアルデヒドフクシン染色により，結合組織内の線維成分を同定すると，膠原線維が終末細気管支周囲の漏出液中に分断されて散在したが，弾性線維は血管周囲や肺胞中隔壁結合組織に連続して認めた（図 7a）。また肺胞腔内の漏出液は，パラフィン包埋した連続切片を血清アルブミン抗体を用いて免疫染色すると，強陽性であることから，漏出血清成分の局在・分布が容易に検討できた（図 7b, c）。

V. おわりに

以上のように生体内凍結技法により，呼吸機能状態下肺組織を任意の時点で停止させた光顕用組織切片像が得られた。さらに右心室内 Qdot 注入によって，肺内小葉間細動脈から毛細血管網を経て，速やかに細静脈へと流入する血行動態像と，その規則的な動静脈の血管配置が可視化された。また，実験的肺水腫モデルでの肺胞腔や中隔壁内血管構築像と合わせて，漏出液の蛋白成分についても，切片上で免疫組織化学的に解析できた。すでに我々は，低温ステー

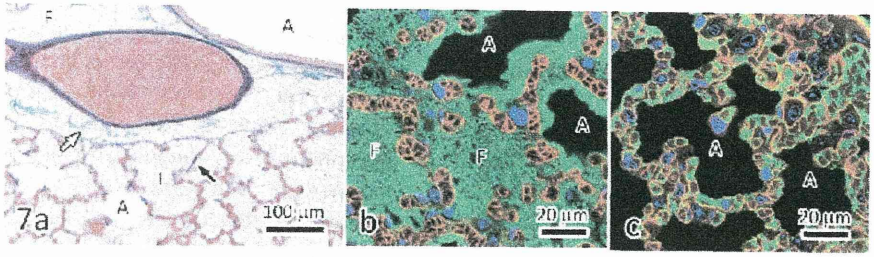

図7．肺水腫（a, b）および正常（c）の生体内凍結肺組織のアルデヒドフクシン染色（a）と免疫染色像（b, c）：肺胞腔に漏出液が認められ，抗原線維が漏出液中に散在している（a）．連続切片で免疫染色すると，肺胞腔に認められる漏出液はアルブミン陽性で，肺胞中隔壁内毛細血管には，赤血球がうっ滞している（b）．正常肺では，肺胞腔にアルブミンは認められない（c）．
白矢印（⇒）：分断された膠原線維（緑色），
黒矢印（➡）：連続する弾性線維（紫色），
A：気道，F：漏出液
（b, c）：緑－アルブミン，赤－アクアポリン1（血管内皮細胞，赤血球），青－DAPI（核）．

ジ上（-150℃）で分子構造に特有な振動波であるラマンスペクトルを解析できるクライオーラマン顕微鏡法を生体内凍結標本に適用することによって，マウス小腸・肝臓血管の流動赤血球内ヘモグロビン酸素飽和度に対応した共鳴ラマンシフト解析で分子構造変化を発表したが[23]，さらに光顕切片作製用の凍結置換固定法と組み合わせることで，種々の血行動態と酸欠状態下臓器組織の時間・空間的な相互関係も明らかにできると考えている。このように生きた動物臓器を反映した機能的形態像が得られるので，生体内蛍光イメージングとのギャップをうめられる一方で，機能的蛍光イメージング法とは異なり，動物臓器の実体として標本ブロック内に保存された物質の組織切片上での種々の解析が可能となった。今後，この生体内凍結技法と蛍光イメージング法等の併用により，さらに種々の生体内分子の動態解析が可能である。

文　献

1) Beigelman-Aubry C, Hill C, Guibal A, Savatovsky J, Grenier PA: Multi-detector row CT and post-processing techniques in the assessment of diffuse lung disease. Radiographics. 25: 1639–1652, 2005.
2) Driehuys B, Cofer GP, Pollaro J, Mackel JB, Hedlund LW, *et al.*: Imaging alveolar-capillary gas transfer using hyperpolarized 129Xe MRI. Proc Natl Acad Sci. 103: 18278–18283, 2006.
3) Gassmann P, Kang ML, Mees ST, Haier J: In vivo tumor cell adhesion in the pulmonary microvasculature is exclusively mediated by tumor cell—endothelial cell interaction. BMC Cancer. 10: 177, 2010.
4) Langheinrich AC, Leithauser B, Greschus S, Von Gerlach S, Breithecker A, *et al.*: Acute rat lung injury: feasibility of assessment with micro-CT. Radiology. 233: 165–171, 2004.
5) Mondy WL, Cameron D, Timmermans JP, De Clerck N, Sasov A, *et al.*: Micro-CT of corrosion casts for use in the computer-aided design of microvasculature. Tissue Eng Part C Methods. 15: 729–738, 2009.
6) Richter T, Bergmann R, Pietzsch J, Kozle I, Hofheinz F, *et al.*: Effects of posture on regional pulmonary blood flow in rats as measured by PET. J Appl Physiol. 108: 422–429, 2010.
7) Ohno S, Terada N, Fujii Y, Ueda H, Takayama I: Dynamic structure of glomerular capillary loop as revealed by an in vivo cryotechnique. Virchows Arch. 427: 519–527, 1996.
8) Ohno S, Terada N, Ohno N, Saitoh S, Saitoh Y, *et al.*: Significance of 'in vivo cryotechnique' for morphofunctional analyses of living animal organs. J Electron Microsc (Tokyo). 59: 395–408, 2010.

9) Saitoh Y, Terada N, Saitoh S, Ohno N, Fujii Y, *et al.*: Three-dimensional reconstruction of living mouse liver tissues using cryotechniques with confocal laser scanning microscopy. J Electron Microsc (Tokyo). 59: 513–525, 2010.
10) Saitoh Y, Terada N, Saitoh S, Ohno N, Fujii Y, *et al.*: Histochemical approach of cryobiopsy for glycogen distribution in living mouse livers under fasting and local circulation loss conditions. Histochem Cell Biol. 133: 229–239, 2010.
11) Shimo S, Saitoh S, Terada N, Ohno N, Saitoh Y, *et al.*: Immunohistochemical detection of soluble immunoglobulins in living mouse small intestines using an in vivo cryotechnique. J Immunol Methods. 361: 64–74, 2010.
12) Terada N, Ohno N, Saitoh S, Saitoh Y, Ohno S: Immunoreactivity of glutamate in mouse retina inner segment of photoreceptors with in vivo cryotechnique. J Histochem Cytochem. 57: 883–888, 2009.
13) Ballou B, Lagerholm BC, Ernst LA, Bruchez MP, Waggoner AS: Noninvasive imaging of quantum dots in mice. Bioconjug Chem. 15: 79–86, 2004.
14) Dickie R, Bachoo RM, Rupnick MA, Dallabrida SM, Deloid GM, *et al.*: Three-dimensional visualization of microvessel architecture of whole-mount tissue by confocal microscopy. Microvasc Res. 72: 20–26, 2006.
15) Ferrara DE, Weiss D, Carnell PH, Vito RP, Vega D, *et al.*: Quantitative 3D fluorescence technique for the analysis of en face preparations of arterial walls using quantum dot nanocrystals and two-photon excitation laser scanning microscopy. Am J Physiol Regul Integr Comp Physiol. 290: R114–123, 2006.
16) Jamieson T, Bakhshi R, Petrova D, Pocock R, Imani M, *et al.*: Biological applications of quantum dots. Biomaterials. 28: 4717–4732, 2007.
17) Larson DR, Zipfel WR, Williams RM, Clark SW, Bruchez MP, *et al.*: Water-soluble quantum dots for multiphoton fluorescence imaging in vivo. Science. 300: 1434–1436, 2003.
18) Michalet X, Pinaud FF, Bentolila LA, Tsay JM, Doose S, *et al.*: Quantum dots for live cells, in vivo imaging, and diagnostics. Science. 307: 538–544, 2005.
19) Terada N, Saitoh Y, Saitoh S, Ohno N, Jin T, *et al.*: Visualization of microvascular blood flow in mouse kidney and spleen by quantum dot injection with "in vivo cryotechnique". Microvasc Res. 80: 491–498, 2010.
20) Jin T, Fujii F, Komai Y, Seki J, Seiyama A, *et al.*: Preparation and characterization of highly fluorescent, glutathione-coated near infrared quantum dots for in vivo fluorescence imaging. Int J Molecu Scie. 9: 2044–2061, 2008.
21) Tiwari A, Snure M: Synthesis and characterization of ZnO nano-plant-like electrodes. J Nanosci Nanotechnol. 8: 3981–3987, 2008.
22) Rimoldi SF, Yuzefpolskaya M, Allemann Y, Messerli F: Flash pulmonary edema. Prog Cardiovasc Dis. 52: 249–259, 2009.
23) Terada N, Ohno N, Saitoh S, Ohno S: Application of "in vivo cryotechnique" to detect erythrocyte oxygen saturation in frozen mouse tissues with confocal Raman cryomicroscopy. J Struct Biol. 163: 147–154, 2008.

PLOS | ONE

RESEARCH ARTICLE

SOX10 Transactivates S100B to Suppress Schwann Cell Proliferation and to Promote Myelination

Sayaka Fujiwara[1], Shinya Hoshikawa[1], Takaaki Ueno[1], Makoto Hirata[1], Taku Saito[2], Toshiyuki Ikeda[1], Hiroshi Kawaguchi[1], Kozo Nakamura[1], Sakae Tanaka[1], Toru Ogata[3]*

1. Departments of Sensory & Motor System Medicine, Faculty of Medicine, University of Tokyo, Tokyo, Japan, **2.** Bone and Cartilage Regenerative Medicine, Faculty of Medicine, University of Tokyo, Tokyo, Japan, **3.** Department of Rehabilitation for the Movement Functions, Research Institute, National Rehabilitation Center for Persons with Disabilities, Saitama, Japan

*ogata-toru@rehab.go.jp

OPEN ACCESS

Citation: Fujiwara S, Hoshikawa S, Ueno T, Hirata M, Saito T, et al. (2014) SOX10 Transactivates S100B to Suppress Schwann Cell Proliferation and to Promote Myelination. PLoS ONE 9(12): e115400. doi:10.1371/journal.pone.0115400

Editor: Petri Kursula, University of Oulu, Finland

Received: July 17, 2014

Accepted: November 21, 2014

Published: December 23, 2014

Data Availability: The authors confirm that all data underlying the findings are fully available without restriction. All relevant data are contained within the paper.

Funding: This study was supported by a Grant-in-aid for Scientific Research from the Japanese Ministry of Education, Culture, Sports, Science, and Technology (#23300204). http://www.jsps.go.jp/english/index.html. This grant has been received by TO. The funders had no role in study design, data collection and analysis, decision to publish, or preparation of the manuscript.

Competing Interests: The authors have declared that no competing interests exist.

Abstract

Schwann cells are an important cell source for regenerative therapy for neural disorders. We investigated the role of the transcription factor sex determining region Y (SRY)-box 10 (SOX10) in the proliferation and myelination of Schwann cells. SOX10 is predominantly expressed in rat sciatic nerve-derived Schwann cells and is induced shortly after birth. Among transcription factors known to be important for the differentiation of Schwann cells, SOX10 potently transactivates the *S100B* promoter. In cultures of Schwann cells, overexpressing SOX10 dramatically induces S100B expression, while knocking down SOX10 with shRNA suppresses S100B expression. Here, we identify three core response elements of SOX10 in the *S100B* promoter and intron 1 with a putative SOX motif. Knockdown of either SOX10 or S100B enhances the proliferation of Schwann cells. In addition, using dissociated cultures of dorsal root ganglia, we demonstrate that suppressing S100B with shRNA impairs myelination of Schwann cells. These results suggest that the SOX10-S100B signaling axis critically regulates Schwann cell proliferation and myelination, and therefore is a putative therapeutic target for neuronal disorders.

Introduction

Schwann cells have recently attracted great attention as a cell source for regenerative therapy for various kinds of neuronal disorders. Therefore, it is now crucial to elucidate the mechanisms of Schwann cell differentiation and function.

Previous studies have clarified the role of various cytokines in Schwann cell proliferation and differentiation [1]. In addition, the developmental expression pattern of Schwann cell differentiation markers such as S100, nerve growth factor receptor (NGFR, also known as p75NTR), myelin associated glycoprotein (MAG), and myelin protein zero (MPZ, also known as P0), as well as transcription factors such as SOX10, paired box 3 (PAX3), POU class 3 homeobox 1 (POU3F, also known as Oct6), and early growth response 2 (EGR2, also known as KROX20) have been extensively studied [2, 3].

SOX family transcription factors are known to be involved in determining cell fate. Among the family members, SOX9 and SOX10 are involved in neural crest cell (NCC) migration and subsequently determining cell fate between neurons and Schwann cells [4–6]. Although the exact role of SOX10 in Schwann cell development still remains elusive, SOX10 is expressed from the early NCC stage through all stages of Schwann cell development and into adulthood [7].

S100 family proteins are abundantly expressed in glial cells, and some of the family members are implicated in a variety of intracellular and extracellular functions [8]. In the central nervous system (CNS), S100B promotes proliferation and inhibits differentiation of astrocytes [9], and increases in S100B are associated with neural diseases such as amyotrophic lateral sclerosis, multiple sclerosis, depression, Alzheimer's disease, and schizophrenia [10–13]. In addition, patients with Down's syndrome caused by chromosome 21 trisomy exhibit excessive expression of S100B, whose gene coding region is located on chromosome 21 [12, 14]. The expression of S100B gradually increases during Schwann cell differentiation [15, 16], and we previously reported that S100B expression is induced by SOX9 in chondrocytes [17]. Some studies point to an association between SOX10 and S100B; for instance, knockdown of SOX10 in Schwannoma cells drastically reduces S100B levels [18]. Waardenburg-Shah syndrome type 4, in which SOX10 mutations are observed, causes myelination disorders and peripheral neuropathy [19, 20]. Hirschsprung disease, also characterized by SOX10 mutations, causes the absence of the myenteric plexus where S100B is usually expressed [21]. In the present study, we identify S100B as one of the transcriptional targets of SOX10 during the differentiation of Schwann cells. We further found that the SOX10-S100B signaling axis regulates the proliferation and myelination of Schwann cells.

Materials and Methods

Cell cultures

All mouse experiments were performed according to the protocol approved by the Animal Care and Use Committee of the University of Tokyo. Carbon dioxide and decapitation were applied to euthanize adult and embryo rats, respectively. Primary rat Schwann cells were isolated and cultured as previously reported [22]. Briefly, we harvested Schwann cells from sciatic nerves of Wistar rats at postnatal day 2 (P2) and cultured the cells in DMEM containing 10% FBS and we added

10 μM AraC to the medium on the next day to eliminate contamination from fibroblasts. After 48 h, we replaced the medium with DMEM containing 3% FBS with 3 μM forskolin and 20 ng/mL neuregulin to expand the cells. We subcultured the cells by re-plating them onto poly-L-lysine-coated plastic dishes before confluence. We used Schwann cells between passages 3 and 7 in all experiments. For retrovirus infection, cells were incubated with DMEM containing retroviral vectors for 2 h, and then the medium was changed to DMEM with 10% FBS and cultured for an additional 48 h. Primary chondrocytes were isolated from the ribs of mouse embryos and cultured in DMEM with 10% FBS as previously described [23].

Luciferase reporter assay

We cloned rat *S100b* promoter region from −1,000 to +200 bp relative to the transcriptional start site into the pGL3-Basic vector (Promega). We created deletion and mutation constructs by PCR. We cultured Schwann cells in medium containing 2 mM forskolin and 2 nM recombinant neuregulin (rh-HRG-1; Genzyme) before the transfection with the constructs and in medium with 2 mM forskolin and without neuregulin after the transfection. We performed luciferase assays with the PicaGene Dual SeaPansy Luminescence Kit (Toyo Ink) and present data as the ratio of the firefly activity to the Renilla activity.

Chromatin immunoprecipitation (ChIP) assays

We performed ChIP assays in primary rat Schwann cells with an EZ ChIP kit (Upstate) as described by the manufacturer. Briefly, we obtained DNA, crosslinked to protein with formaldehyde, and sheared the DNA by pulsed ultrasonication. For immunoprecipitation, we used an anti-SOX10 antibody (Santa Cruz) or a rabbit IgG antibody (negative control). Primer sets, spanning the identified response element, ranged from −421 to −157 bp (site AB), from −421 to −224 bp (site A), from −285 to −46 bp (site B), and from −78 to +169 bp (site D) relative to the transcriptional start site.

Plasmids and viral vectors

We prepared shRNA vectors for rat *S100b*, rat *Sox10*, *GFP* and *luciferase* in piGENE mU6 vectors (iGENE Therapeutics). The sequence information of oligonucleotides synthesized for RNAi is available upon request. We subcloned the mouse U6 gene promoter and shRNA sequence from piGENE mU6 vectors into pMX–puro vectors to generate retroviral vectors as previously described [24].

Real-time RT-PCR

We isolated total RNA from primary rat Schwann cells using Isogen (Wako) and an RNeasy Mini Kit (Qiagen). We used 1 μg of total RNA for a reverse transcription reaction with the QuantiTect Reverse Transcription kit (Qiagen) to

generate single-stranded cDNA. We performed real-time PCR assays based on SYBR Green detection with the ABI Prism 7000 Sequence Detection system (Applied Biosystems). Copy numbers of target gene mRNA in each total RNA were calculated by reference to standard curves and were adjusted to the standard total RNA (Applied Biosystems), using beta-actin for normalization [17, 25]. We observed that the Ct values of the standard vector samples of each gene were similar to each other. All reactions were run in triplicate. Primer sequence information is available upon request.

Western blotting

We lysed rat Schwann cells in M-Per mammalian protein extraction reagent (Pierce) containing a complete mini protease inhibitor cocktail tablet (Roche). For immunoblot analysis, lysates were fractionated by SDS-PAGE and transferred onto PVDF membranes (BIO-RAD). The membranes were incubated with an antibody to S100B (SH-B1, Sigma-Aldrich), SOX10 (N-20, Santa Cruz), or β-actin (Sigma-Aldrich). The immunoblots were developed by using the ECL system (Amersham Biosciences).

Cell proliferation assay

We seeded Schwann cells at 10^3 cells per well in a 96-well plate and evaluated cell proliferation by the modified MTT method designated WST-8 as indicated in the manufacture's instruction (Dojindo Laboratories) at the indicated time point. The absorbance of the product at the 490-nm wavelength was measured using an automated microplate reader (Bio-Tek Instruments). For BrdU detection analysis, we labeled the Schwann cells with 10 μM BrdU (Sigma) for 18 h and the cells were stained using a BrdU Immunohistochemistry System (Calbiochem). The cells were counterstained with the nuclear stain DAPI. The percentage of cells that had incorporated BrdU was quantified by determining the ratio of BrdU-positive nuclei and the total number of nuclei in 15 systematically sampled microscope fields.

Myelination assay

We used dorsal root ganglion (DRG) neuronal coculture with Schwann cells as previously described [26]. Briefly, we isolated DRGs from embryonic rats at embryonic day (E) 15, dissociated with trypsin, and seeded them on 12-mm dishes coated with collagen type I at 200,000 cells per well. Non-neuronal cells were removed by treating cultures with C media (MEM, 10% FBS, 0.4% glucose, and 100 ng/mL 2.5S NGF) supplemented with 5-fluorodeoxyuridine, uridine, and AraC (10 μM) or with C media alone every 2–3 days alternately for 10 days. For myelination, 250,000 retrovirally-infected Schwann cells were seeded onto DRG cultures in DMEM/F12 medium with N2 supplement (Gibco) and 50 ng/mL NGF and kept for several days until Schwann cells populated axons. The medium was

then switched to C media with 50 ng/mL ascorbic acid to promote myelination. Cocultures were kept for 2 weeks and then fixed with 4% paraformaldehyde. Anti-myelin basic protein (MBP) and anti-Tuj1 antibodies diluted at 1:200 in TBST with 3% BSA were applied overnight at room temperature. Fluorescently-labeled secondary antibodies, Alexa Fluor 488 or 568, diluted at 1:500 in TBST were then added to observe myelin-forming Schwann cells with fluorescence microscopy. The number of myelin-forming Schwann cells was counted by surveying 20 fields at 200 × magnification from three independent experiments and expressed as a percentage ratio of control cultures.

Statistical analysis

Group means were compared by ANOVA, and significance of differences were determined by post-hoc testing using Bonferroni's method.

Results

Expression of *Sox10* and *S100b* during Schwann cell differentiation

As shown in Fig. 1, *Sox10* was predominantly expressed in primary rat Schwann cells as compared to *Sox9* (Fig. 1A), while *Sox9* was highly expressed in primary rat rib chondrocytes as compared to *Sox10* (Fig. 1B). We then analyzed the expression of *Sox10* and other factors known to be involved in Schwann cell development in rat DRG at E15 and rat sciatic nerve at 2, 7, and 12 days after birth. *Sox10* expression markedly increased after birth and gradually decreased thereafter (Fig. 1C). The expressions of *S100b*, *Mpz*, *Mag*, *Periaxin* (*Prx*), and *Mbp* were induced after birth following *Sox10* induction (Fig. 1C).

Regulation of S100B by SOX10

To investigate the regulation of S100B by SOX10 in Schwann cells, we retrovirally overexpressed SOX10 in primary rat sciatic Schwann cells and rat osteosarcoma ROS cells (Fig. 2A, top). The expression level of S100B was significantly increased in SOX10-overexpressing Schwann cells (Fig. 2A, bottom and B), as well as in SOX10-overexpressing ROS cells (Fig. 2C). Conversely, when we suppressed SOX10 expression with a specific shRNA, the expression of S100B and Mpz was significantly suppressed (Fig. 3). These results suggest that SOX10 regulates S100B expression in Schwann cells.

We then analyzed the promoter activity of human *S100B* using human HeLa cells transfected with a luciferase reporter gene construct containing a 5′-flanking sequence from −1,000 to +200 bp relative to the transcriptional start site of *S100B*. Among the transcription factors known to regulate Schwann cell differentiation, such as EGR2, POU3F, PAX3, and SOX10, SOX10 most potently enhanced transcriptional activity (Fig. 4A). Deletion analysis by a series of 5′-deletion constructs identified the location of the SOX10 response element between

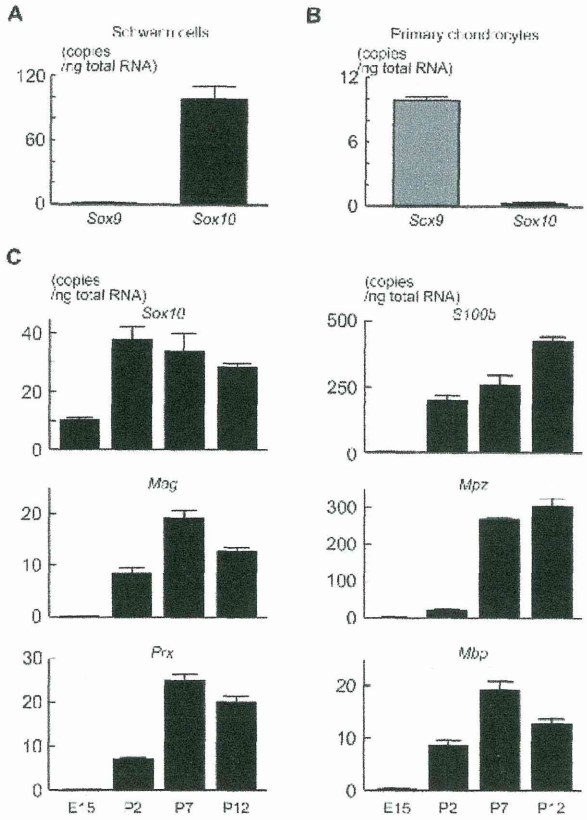

Fig. 1. Expression pattern of *Sox10* and other differentiation markers in Schwann cells. (A and B) Comparison of expression level between *Sox10* and *Sox9* in primary rat sciatic nerve Schwann cells and primary rat rib chondrocytes. (C) Time course of mRNA levels of Schwann cell differentiation markers determined by real-time RT-PCR analysis during rat perinatal stages. All experiments were repeated independently three times with data shown as the mean (bars) ± SEM (error bars).

doi:10.1371/journal.pone.0115400.g001

−334 and −240-bp (Fig. 4B). This region has been reported as a Sox10 binding site in ChIP-Seq analysis by Srinivasan et al. [27] and contains three putative consensus sites for SOX10, each of which was highly conserved among species like human, rat, and mouse (sites A, B, and C) (Fig. 4C). Site-directed mutagenesis of sites A and B but not of site C significantly suppressed transactivity of SOX10 (Fig. 4D). Deletion analysis using a 3′-deletion construct and site-directed mutagenesis demonstrated another putative SOX10-response element in the first intron (site D) (Fig. 5A–5B). A ChIP assay demonstrated the direct binding of SOX10 to the SOX motifs in sites A, B, and D (Fig. 5C).